Pathological Vascular Invasion and Tumor Differentiation Predict Cancer Recurrence in Stage IA Non–Small-Cell Lung Cancer After Complete Surgical Resection

Yoshihisa Shimada, MD, PhD, Hisashi Saji, MD, PhD,* Koichi Yoshida, MD, PhD,* Masatoshi Kakihana, MD, PhD,* Hidetoshi Honda, MD, PhD,* Masaharu Nomura, MD, PhD,*† Jitsuo Usuda, MD, PhD,* Naohiro Kajiwara, MD, PhD,* Tatsuo Ohira, MD, PhD,* and Norihiko Ikeda, MD, PhD**

Introduction: The appropriate therapeutic strategy and postoperative management for patients with stage IA non–small-cell lung cancer (NSCLC) still remain a matter of debate because of the prognostic heterogeneity of this population, including the risk of cancer recurrence. The objective of the current study was to identify the clinicopathological factors that affect overall prognosis and cancer recurrence of stage IA NSCLC.

Methods: We reviewed the data of 532 patients in whom complete resection of stage IA NSCLC had been performed. Overall survival and recurrence-free proportion (RFP) were estimated using the Kaplan–Meier method. RFP was estimated from the date of the primary tumor resection to the date of the first recurrence or last follow-up. We performed univariate and multivariate analyses to determine the independent prognostic factors.

Results: On multivariate analyses, three variables were shown to be independently significant recurrence risk factors: histological differentiation (hazard ratio [HR] = 1.925), blood-vessel invasion (HR = 1.712), and lymph-vessel invasion (HR = 1.751). On subgroup analyses combining these risk factors, the 5-year RFP was 91.3% for patients with no risk factors, 79.5% for those with either poorly differentiated carcinoma or vascular invasion, ($p < 0.001$ for both), and 62.9% for those with both poorly differentiated carcinoma and vascular invasion ($p = 0.068$).

Conclusion: These results indicated that vascular invasion and tumor differentiation have a significant impact on the prediction of cancer recurrence in patients with stage IA NSCLC. Patients with these predictive factors of recurrence may be good candidates for adjuvant chemotherapy.

Key Words: Prognostic factor, Non–small-cell lung cancer, Recurrence, Stage IA, Vascular invasion, Tumor differentiation.

(*J Thorac Oncol.* 2012;7: 1263–1270)

*First Department of Surgery, and †Diagnostic Pathology, Division, Tokyo Medical University Hospital, Shinjyuku-ku, Tokyo, Japan.

Disclosure: The authors declare no conflicts of interest.

Address for correspondence: Yoshihisa Shimada, MD, PhD, First Department of Surgery, Tokyo Medical University, 6-7-1 Nishishinjuku, Shinjyuku-ku, Tokyo, 160-0023, Japan. E-mail: zenkyu@za3.so-net.ne.jp

ISSN: 1556-0864/12/0708-1263

The tumor, node, metastasis (TNM) staging system for non–small-cell lung cancer (NSCLC) is currently the best confirmed predictor of survival and guide for treatment. NSCLC patients with pathologic stage IA disease have the best chance of survival, and resection is standard in such cases. However, even after curative resection, the 5-year survival rate is between 80% and 87% in pathologic stage IA patients as shown in large-scale Japanese lung cancer studies,[1–3] and recent data from the lung cancer staging project of the International Association for the Study of Lung Cancer revealed a 5-year survival rate of 73% for pathological stage IA patients.[4] Therefore, up to 10% of patients with stage IA NSCLC have recurrence after surgery, even in cases with early-stage disease.

Many studies of resected specimens have been performed to determine various clinicopathological prognostic factors other than the pathologic stage for these patients, such as sex, age,[5] smoking history,[6] serum level of carcinoembryonic antigen (CEA),[7] extent of operation,[5] tumor size, vascular invasion,[7–18] and the grade of differentiation of the tumor.[14,17,19] Patients, including those with stage IA NSCLC, who have such factors may be good candidates for receiving systemic therapy such as adjuvant chemotherapy. The objective of the present study was to identify the clinicopathological factors that affect overall prognosis and cancer recurrence of stage IA NSCLC in a single institution.

PATIENTS AND METHODS

Patients

From January 1990 to December 2007, a total of 1973 patients underwent complete pulmonary resection for NSCLC at our hospital. Complete resection was defined as cancer-free surgical margins both grossly and histologically. All the patients underwent radical surgical resection and systematic mediastinal lymph node dissection. Of these, 674 patients with consecutive pathologic stage IA NSCLC were identified in our departmental database. The number of resected lymph nodes ranged from one to 49, with a mean of 15. We excluded 142 patients who had undergone preoperative chemotherapy

or radiotherapy (n = 17), postoperative treatment including chemotherapy or chemoradiotherapy (n = 105), and those who had low-grade malignant tumors including carcinoids, mucoepidermoid carcinomas, or adenoid cystic carcinomas (n = 20). The remaining 532 patients comprised the subjects of this study.

Preoperative evaluation included physical examination, chest radiography, computed tomography (CT) of the chest and abdomen, bone scintigraphy, blood examination, and since the early 2000s, positron-emission tomography (PET) scan (recently performed as integrated PET-CT scan). Most patients were postoperatively evaluated by physical examination, chest radiography, and CT of the chest and abdomen to confirm relapse. In some patients, we used PET-CT, magnetic resonance imaging or bone scintigraphy to detect recurrence. The disease stage was determined in accordance with the 7th edition of the TNM classification for lung and pleural tumors.[20]

Histopathology

The available pathology slides from all 532 surgical specimens were reviewed in this study. After fixing the specimens with either 10% formalin and embedding them in paraffin, serial 4-μm sections were stained with hematoxylin and eosin and by elastica van Gieson (EvG) to visualize elastic fibers. Histologic subtypes of lung cancer were determined according to World Health Organization classification.[21] The histological tumor grade was categorized as well-differentiated, moderately differentiated, or poorly differentiated carcinoma according to the degree of structural and cytologic atypia.

Blood vessels were identified by the presence of erythrocytes in the lumen and/or an endothelial cell lining and/or the presence of elastic tissue around larger vessels. Sections stained by EvG were examined for the presence of blood-vessel invasion. The presence of blood-vessel invasion was determined by identifying conspicuous clusters of intravascular cancer surrounded by an elastic layer.

Lymph-vessel invasion was determined to be present when tumor cells floating in lymphatic vessels with no supporting smooth muscles or elastic fibers were identified. We confirmed that lumens within the bronchovascular bundle, subpleural, and intralobular pleural space were lymphatic vessels by immunostaining with anti-D2-40 antibody.

Data Collection

Clinical characteristics were retrieved from available clinical records. The following clinicopathological factors were assessed in the retrospective prognostic analysis: age (dichotomized at the median age of 64 years), sex, smoking status, preoperative serum CEA level (cutoff at the normal upper limit of 5 ng/ml), tumor size, tumor differentiation (well or moderate versus poor), blood-vessel invasion (absence versus presence), lymph-vessel invasion (absence versus presence), histology (adenocarcinoma versus other), tumor laterality, and extent of resection (single-lobe lobectomy versus more extensive resection; bilobectomy or pneumonectomy).

Statistical Analysis

Overall survival (OS) was measured from the date of surgery to the date of death from any cause or the date on which the patient was last known to be alive. The length of the recurrence-free period was calculated in months from the date of resection to the date of the first recurrence or last follow-up showing no recurrence. To calculate the recurrence-free proportion (RFP), patients who died without recurrence or who were known to have no recurrence at the date of last contact were censored. OS and RFP curves were plotted using the Kaplan–Meier method, and differences in variables were determined using the log-rank test. Categorical comparison was performed using the Pearson

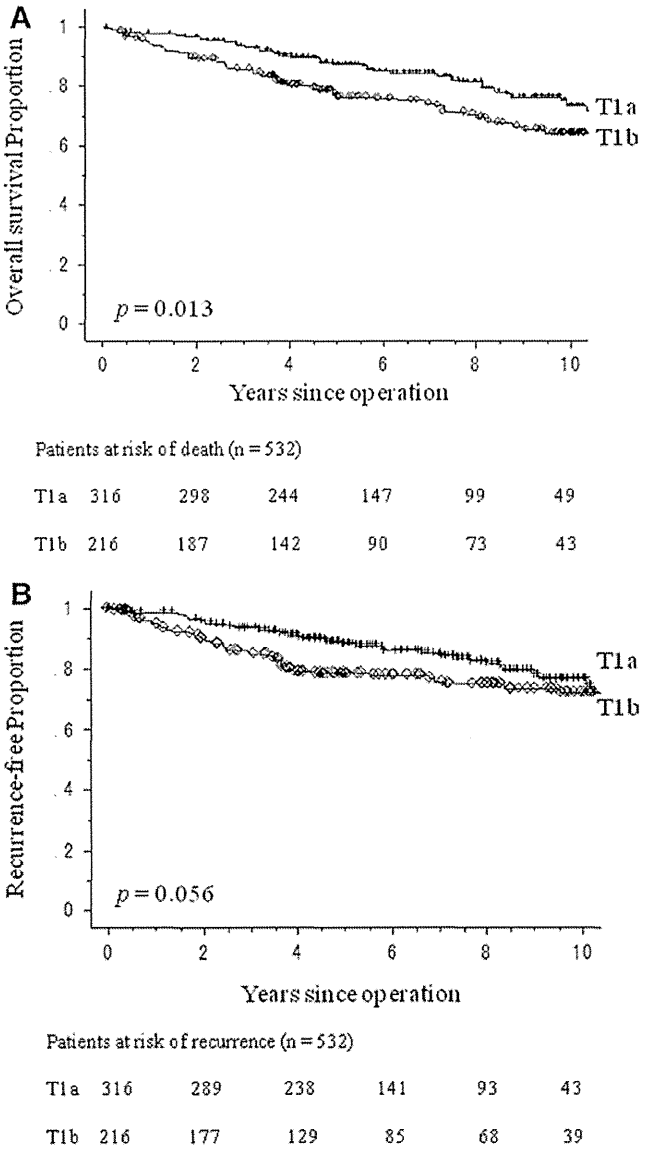

FIGURE 1. *A*, Overall survival curves of patients with T1a or T1b disease. *B*, Recurrence-free proportion curves of patients with T1a or T1b disease.

χ^2 test. Multivariate analyses were performed using the Cox proportional hazards regression model. All tests were two-sided, and p values of less than 0.05 were considered to indicate a statistically significant difference. Statview 5.0 software (SAS Institute Inc., Cary, NC) was used for statistical analyses. Data collection and analyses were approved and the need to obtain written informed consent from each patient was waived by the institutional review board of our institution.

RESULTS

The median follow-up for survivors was 5.1 years. Figure 1*A* and *B* show the OS and RFP curves of 316 patients with T1aN0M0 NSCLC and 216 patients with T1bN0M0 NSCLC. For those patients with T1aN0M0 NSCLC and those with T1bN0M0 NSCLC, the 5-year OS rates were 87.1% and 77.2% ($p = 0.013$), respectively, whereas the 5-year RFPs were 88.6% and 78.6% ($p = 0.056$), respectively.

Table 1 shows the 5-year OS proportions and RFPs according to the clinicopathological characteristics of the stage IA NSCLC patients. On univariate analysis, nine variables were found to be significantly associated ($p < 0.05$) with poorer OS: older age, male sex, smoking history, T1b, poorly differentiated carcinoma, blood-vessel invasion, lymph-vessel invasion, nonadenocarcinoma, and type of surgery (bilobectomy or pneumonectomy). For RFP, five variables (male sex, poorly differentiated carcinoma, blood-vessel invasion, lymph-vessel invasion, and nonadenocarcinoma) were identified as statistically significant factors on univariate analysis.

A multivariate Cox proportional hazards model demonstrated that older age (hazard ratio [HR] = 1.936; $p < 0.001$), male sex (HR = 2.096; $p = 0.005$), tumor size (HR = 1.501; $p = 0.045$), poorly differentiated carcinoma (HR = 1.632; $p = 0.028$), lymph-vessel invasion (HR = 1.579; $p = 0.042$), and nonadenocarcinoma (HR = 1.704; $p = 0.016$) were statistically significant predictors of OS (Table 2). Poorly differentiated carcinoma (HR = 1.925; $p = 0.006$), blood-vessel invasion (HR = 1.712; $p = 0.020$), and lymph-vessel invasion (HR = 1.751; $p = 0.017$) were identified as statistically significant predictors of cancer recurrence (Table 3). Figures 2*A*, *B*, and *C* show the RFP curves of patients with stage IA NSCLC according to tumor differentiation, blood-vessel invasion, and lymph-vessel invasion, respectively. Table 4 shows the results of 5-year RFP of patients in each T subclassification (T1a and T1b) according to these significant predictors of cancer recurrence.

Subgroup analysis with a combination of these recurrence predictive factors in the patients with stage IA NSCLC revealed 5-year RFPs of 91.3%, 79.5%, and 62.9% for patients with no risk factor, poorly differentiated carcinoma or vascular invasion (blood-vessel invasion or lymph-vessel

TABLE 1. Patient Characteristics and Univariate Analysis of Survival and Recurrence

Variable	No. of Patients	5-Yr OSP (%)	p Value	5-Yr RFP (%)	p Value
Age (yrs: median 64)					
< 64	279	88.9		84.2	
≥ 64	253	76.6	< 0.001	85.3	0.946
Sex					
Male	290	77.7		81.4	
Female	242	89.6	< 0.001	88.4	0.009
Smoking status					
Ever smoker	279	81.5		82.6	
Never smoker	253	84.9	0.039	86.8	0.102
CEA (ng/ml: NUL of 5)					
< 5	447	83.7		85.2	
≥ 5	59	75.9	0.108	77.2	0.212
Tumor size					
T1a (≤ 2.0 cm)	316	87.1		88.6	
T1b (≥ 2.1 cm)	216	77.2	0.013	78.6	0.056
Differentiation					
Well or moderate	425	86.4		87.7	
Poor	96	71.4	< 0.001	71.8	< 0.001
Blood-vessel invasion					
Absent	402	86.2		88.1	
Present	116	72.1	0.002	71.3	< 0.001
Lymph-vessel invasion					
Absent	392	85.4		87.1	
Present	122	76.4	0.003	76.1	0.001
Histology					
Adenocarcinoma	439	86.6		86.6	
Nonadenocarcinoma	93	66.3	< 0.001	74.3	< 0.001
Tumor laterality					
Right	357	82.9		84.3	
Left	175	83.6	0.685	85.4	0.732
Type of surgery					
Single-lobe lobectomy	510	84.0		84.5	
More extensive resection (more than bilobectomy)	22	66.7	0.046	88.7	0.946

OSP, overall survival proportion; RFP, recurrence-free proportion; NUL, normal upper limit; CEA, preoperative serum carcinoembryonic antigen level.

TABLE 2. Multivariate Cox Proportional Hazards Regression Analysis of Overall Survival

Variable	Risk Factors	Hazard Ratio	95% Confidence Interval	p Value
Age	≥ 64	1.936	1.314–2.852	< 0.001
Sex	Male	2.096	1.251–3.510	0.005
Smoking status	Ever smoker	1.219	0.781–1.901	0.383
Tumor size	T1b (≥ 2.1 cm)	1.501	1.009–2.233	0.045
Differentiation	Poor	1.632	1.054–2.527	0.028
Blood-vessel invasion	Present	1.169	0.749–1.827	0.492
Lymph-vessel invasion	Present	1.579	1.017–2.449	0.042
Histology	Nonadenocarcinoma	1.704	1.103–2.632	0.016
Type of surgery	More extensive resection (more than bilobectomy)	1.981	0.984–3.984	0.055

TABLE 3. Multivariate Cox Proportional Hazards Regression Analysis of Cancer Recurrence

Variable	Risk Factors	Hazard Ratio	95% Confidence Interval	*p* Value
Sex	Male	1.171	0.747–1.834	0.492
Differentiation	Poor	1.925	1.210–3.063	0.006
Blood-vessel invasion	Present	1.712	1.088–2.694	0.020
Lymph-vessel invasion	Present	1.751	1.103–2.779	0.017
Histology	Nonadenocarcinoma	1.615	0.994–2.623	0.053

invasion), and both poorly differentiated carcinoma and vascular invasion, respectively (Fig. 3*A*). The differences in RFP were statistically significant between patients without any risk factors (A group) and those with poorly differentiated carcinoma or vessel invasion (B group) ($p < 0.001$). The 5-year RFP of patients with both poorly differentiated carcinoma and vascular invasion (C group) tended to be unfavorable compared with that of patients in the B group, but the difference was not statistically significant ($p = 0.068$). In patients with T1a, the 5-year RFP of patients without any risk factors (A group) was statistically different from that of patients with poorly differentiated carcinoma or vessel invasion (B group) (92.0% versus 83.7% in A and B, respectively; $p = 0.002$), whereas

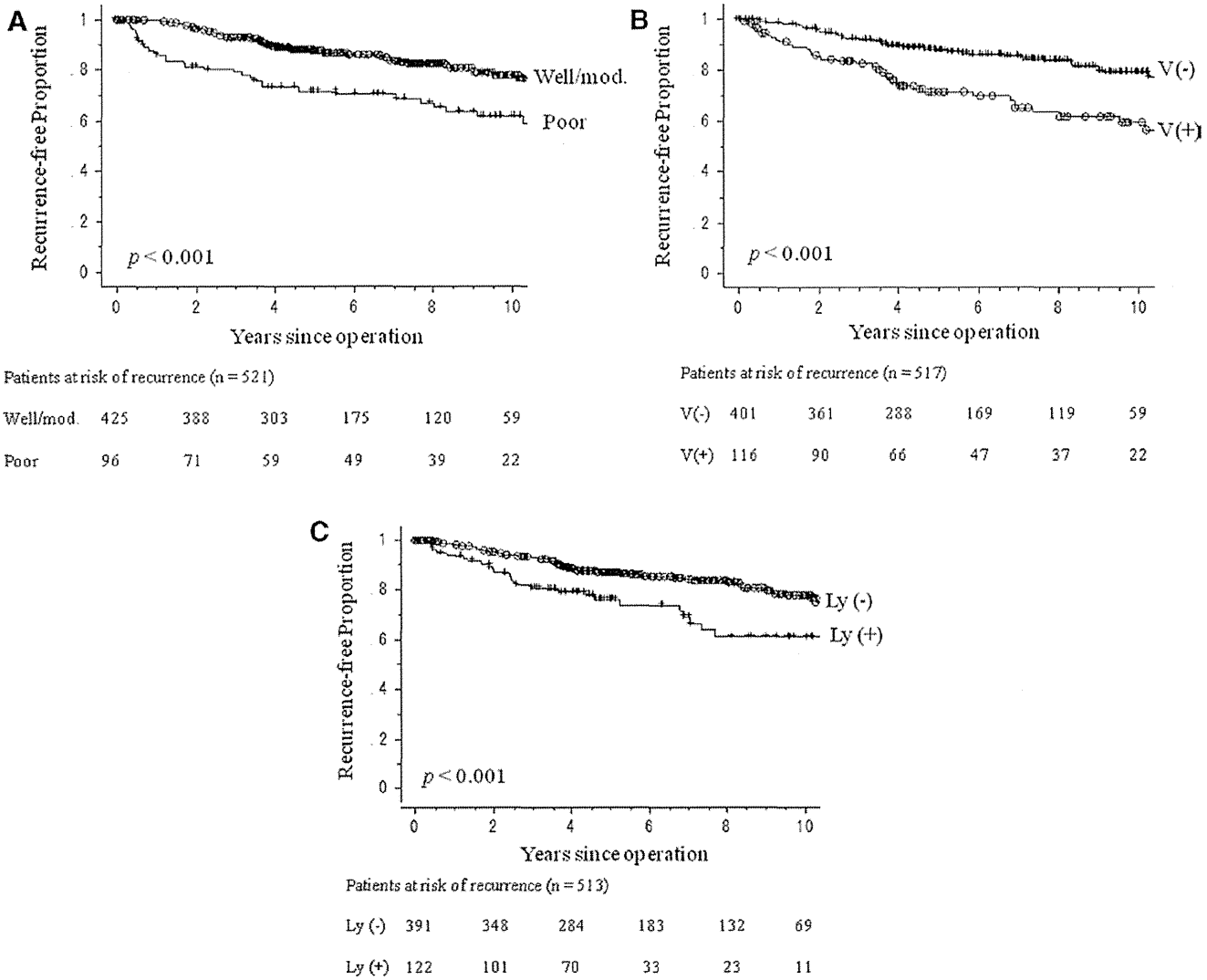

FIGURE 2. *A*, Recurrence-free proportion curves according to tumor differentiation. *B*, Recurrence-free proportion curves according to blood-vessel invasion. *C*, Recurrence-free proportion curves according to lymph-vessel invasion.

TABLE 4. 5-Year Recurrence-Free Proportion for Each T Subclassification According to Histological Grade and Vascular-Invasion Status

T-Factor category	No. of Patients	5-Yr RFP (%)	*p* Value
T1a (≤ 2.0 cm)			
Well/mod.	249	90.3	
Poor	60	83.8	0.126
T1b (≥ 2.1 cm)			
Well/mod.	176	83.7	
Poor	36	51.3	< 0.001
T1a (≤ 2.0 cm)			
BVI (−)	265	90.2	
BVI (+)	44	77.5	0.005
T1b (≥ 2.1 cm)			
BVI (−)	137	83.8	
BVI (+)	72	67.0	0.011
T1a (≤ 2.0 cm)			
LVI (−)	252	90.2	
LVI (+)	54	79.4	0.003
T1b (≥ 2.1 cm)			
LVI(−)	140	81.4	
LVI (+)	68	73.2	0.181

RFP, recurrence-free proportion; Well/mod., well- or moderately differentiated carcinoma; Poor, poorly differentiated carcinoma; BVI, blood-vessel invasion; LVI, lymph-vessel invasion.

no significant difference was shown between patients in the B group and those with both poorly differentiated carcinoma and vascular invasion (C group; 79.4% at 5-year RFP for C group; $p = 0.812$) (Fig. 3*B*). The RFP curves for T1b patients of the A, B, and C groups were shown in Fig. 3*C*. The differences in recurrence were statistically significant between A and B (89.6% versus 75.1% at 5-year RFP in A and B, respectively; $p = 0.006$), B and C (43.3% at 5-year RFP for the C group; $p = 0.002$).

We tested for a correlation between histological grade or vascular-invasion status and clinicopathological variables in stage IA patients. A comparison of variables between well- or moderately differentiated carcinoma and poorly differentiated carcinoma groups showed that a statistically significant difference in the prevalence of poorly differentiated carcinoma was seen in patients of male sex ($p < 0.001$), those who were smokers ($p < 0.001$) those in whom vascular invasion was present ($p < 0.001$), and those who had nonadenocarcinoma histology ($p < 0.001$). Vascular invasion was significantly associated with male sex ($p = 0.035$), smoking ($p = 0.001$), T1b ($p < 0.001$), and poorly differentiated carcinoma ($p < 0.001$) (data not shown).

Table 5 shows the number of patients with recurrence and their initial recurrence pattern according to histological grade and vascular-invasion status. The proportion of patients who developed distant metastases was higher in these recurrence predictive factor positive populations than in the negative populations (histological grade; $p = 0.048$, vascular invasion; $p = 0.024$).

DISCUSSION

We set out to identify the clinicopathological factors that affect overall prognosis and cancer recurrence of stage IA NSCLC. Curative surgical resection is the most effective therapy for patients with stage IA NSCLC. However, a considerable number of patients develop recurrence, which results in cancer death. Previous studies have reported the following factors to be associated with a poor prognosis in patients with stage IA NSCLC: tumor size,[5] preoperative serum CEA level,[7] lymph-vessel invasion,[18] blood-vessel invasion,[7,13–15,17] and histological grade.[14,17,19] In addition, according to the Surveillance, Epidemiology, and End Result Program database, age, sex, and extent of resection are also important prognostic factors.[22] However, prognostic factors such as age and sex do not accurately predict or explain recurrence in patients with stage IA NSCLC. Therefore, we focused on the risk factors for recurrence and unfavorable OS in the present study. When describing the survival experience of a group of patients, the OS parameter is typically used. However, OS is affected by death resulting from causes other than lung cancer itself, including complications and comorbidities, and is considered to be affected by treatment after relapse. For example, epidermal growth factor receptor tyrosine kinase inhibitors are highly effective against mutated epidermal growth factor receptor recurrent NSCLC patients, suggesting potential improvements in postoperative survival regardless of surgery effect. Therefore, in evaluating pure surgical impact on the natural history of early-stage NSCLC, we consider that RFP may be a better prognostic indicator than OS. On multivariate analyses, we identified five independently significant predictors for poor prognosis: older age (HR = 1.936), male sex (HR = 2.096), tumor size (HR = 1.501), poorly differentiated carcinoma (HR = 1.632), lymph-vessel invasion (HR = 1.579), and nonadenocarcinoma (HR = 1.704); we also identified three predictors of recurrence: poorly differentiated carcinoma (HR = 1.925), blood-vessel invasion (HR = 1.712), and lymph-vessel invasion (HR = 1.751). The present study showed that independent predictive factors of poor survival were slightly different from predictive factors of recurrence.

Several authors reported that patients with poor differentiated carcinomas after resection had a higher risk of recurrence and death.[14,23,24] Although the histological grading system may provide useful information in defining the aggressiveness of tumors and has a significant impact on the survival of patients,[19] the four-tiered system of grading (well-differentiated, moderately differentiated, poorly differentiated, and undifferentiated carcinomas) for lung cancer is assumed to lack objectivity, because no original criteria have been developed for standardizing lung cancer histology. However, the current result indicates that poor differentiation contributes to unfavorable clinical outcome, suggesting that this factor may be a useful indicator of a need for postoperative adjuvant chemotherapy in patients with stage IA NSCLC. Consistent grading criteria need to be established for reproducible assessment.

Blood-vessel invasion is considered to be a fundamental step in hematogenous metastasis. The presence of blood-vessel invasion was previously found to be a strong

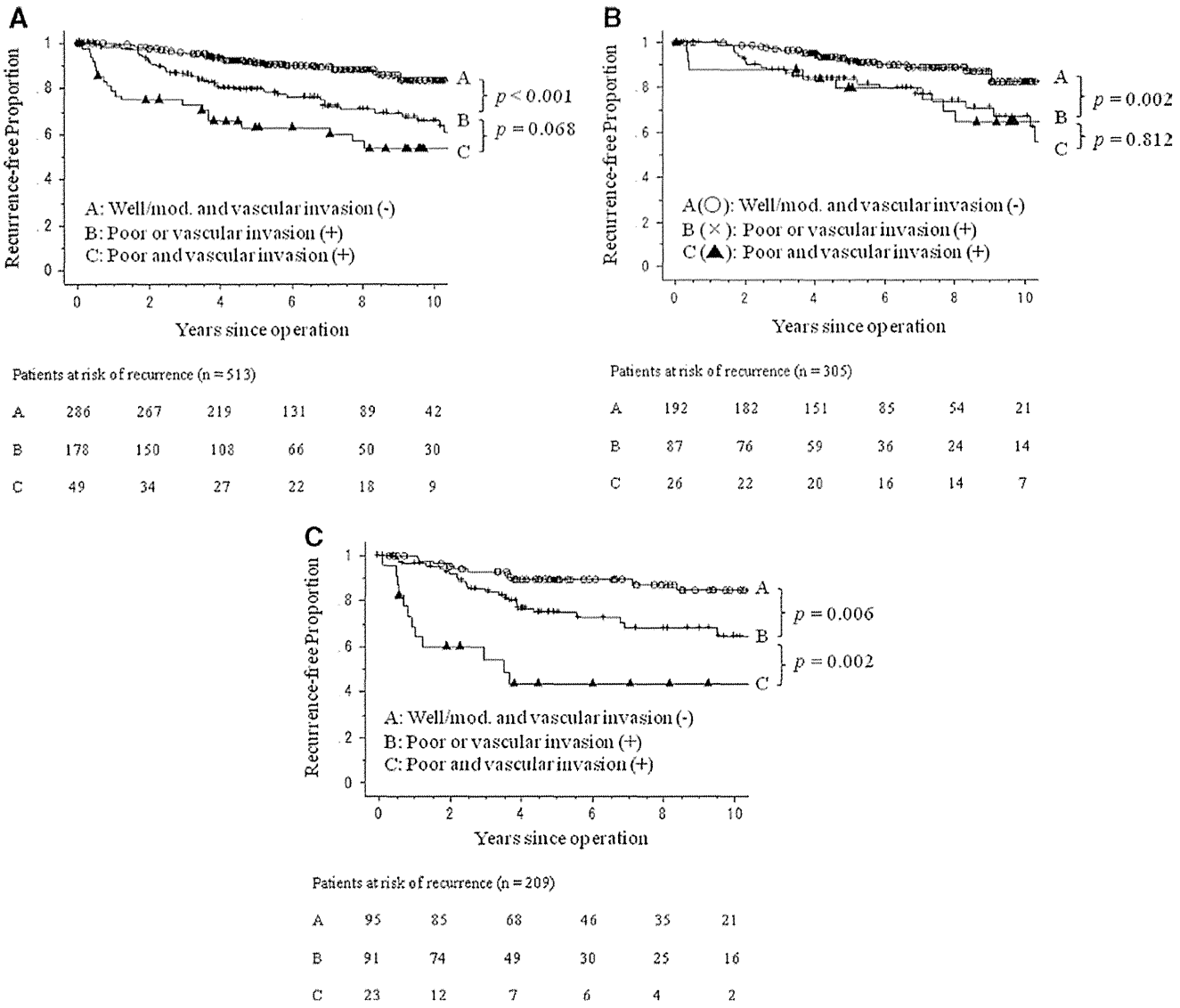

FIGURE 3. *A*, Recurrence-free proportion curves for all stage IA; *B*, T1a; and *C*, T1b patients with well- or moderately differentiated carcinoma and no vascular invasion (curve A), poorly differentiated carcinoma or vascular invasion (curve B), and both poorly differentiated carcinoma and vascular-invasion (curve C).

independent unfavorable prognostic factor, and vascular invasion should be considered for inclusion in the staging criteria and indications for adjuvant chemotherapy.[10,11,13] Fujisawa et al.[25] demonstrated that blood-vessel invasion is a very important prognostic factor in resected NSCLCs with intrapulmonary metastasis, and may correlate with the anatomical aspect of pulmonary metastasis. The current study also suggests that the presence of blood-vessel invasion is a significant risk factor for recurrence in stage IA NSCLC patients.

To identify blood-vessel invasion more accurately, we used hematoxylin and eosin and EvG stains to visualize elastic fibers in all cases. We recommend the routine use of elastic stains in the pathological evaluation of lung cancer, not only for the determination of visceral pleural invasion but also for the determination of blood-vessel invasion, particularly in patients with stage IA NSCLC.

Lymph-vessel invasion has been reported to be an independent indicator of cancer invasiveness and poor prognosis in most studies that included this factor in their analyses.[9,18,26,27] The present study shows that as it is for histological grade, lymph-vessel invasion was a significant predictor of both poor prognosis and cancer recurrence, surpassing tumor size in pathologic stage IA NSCLC.

Recent randomized controlled trials have demonstrated the usefulness of postoperative adjuvant chemotherapy in stage IB to IIIA NSCLC patients who have undergone complete resections.[28–30] Although surgery alone remains the

TABLE 5. Initial Observed Cancer Recurrence Patterns of Patients According to Histological Grade and Vascular-Invasion Status

Initial Recurrence Pattern	Tumor Differentiation			Vascular Invasion		
	Well/ mod.	Poor	*p* Value	Absent	Present	*p* Value
Overall (%)	425 (82)	96 (18)		340 (65)	180 (35)	
Patients with recurrence (%)	64 (15)	35 (36)		46 (14)	53 (29)	
Local recurrence only	24 (38)	9 (25)	0.048	19 (41)	14 (26)	0.025
Distant recurrence	39 (62)	27 (75)		27 (59)	39 (74)	

Well/mod., well- or moderately differentiated carcinoma; Poor, poorly differentiated carcinoma.

standard treatment for patients with stage IA NSCLC, larger studies on resected cases comparing uracil-tegafur adjuvant chemotherapy versus observation showed that uracil-tegafu-rimproved survival for patients with stage I adenocarcinoma, and also showed a clear survival benefit in the T1-disease subgroup of patients with a tumor of diameter more than 2 cm.[31,32] However, tumor size might not be the only factor found to have a benefit on adjuvant chemotherapy after complete resection of stage IA NSCLC. In the present study, when we divided the study population into A (patients without any risk factors), B (those with either poorly differentiated carcinoma or vascular invasion), and C (those with both poorly differentiated carcinoma and vascular invasion) groups, the 5-year RFP of all stage IA patients were 91.3%, 79.5%, and 62.9%, respectively. In particular, the subgroup analysis of patients with stage IA disease stratified by tumor size showed a 5-year RFP of 43.3% for the T1b C group. These results indicated high-risk small-tumor N0 patients, identified by factors other than tumor size, such as tumor differentiation and vascular invasion, may be good candidates for adjuvant chemotherapy.

This study has limitations and biases that should be mentioned. As a retrospective single-institute study, patient-selection bias and time-trend bias regarding the diagnosis for cancer recurrence might be inevitable compared with multi-institutional prospective study. Moreover, the definition of an ipsilateral lung metastasis as a local recurrence also generated inherent bias while allowing the differentiation of a new primary lung cancer from a recurrent NSCLC.

The anatomical extent of disease, as described by the TNM for lung and pleural tumors, remains the most powerful prognostic instrument in NSCLC. A challenge for the future will be to integrate the TNM with specific pathological factors, such as vascular-invasion status or tumor differentiation, to create a composite prognostic index for NSCLC.

CONCLUSION

Even though most patients comprised an early-staging subset, those with stage IA NSCLC comprised a heterogeneous group with different prognoses and risk of cancer recurrence. The current study demonstrates that vascular-invasion status and tumor differentiation were far more powerful recurrence predictive factors than tumor size, and this information can be useful for the selection of the appropriate therapeutic strategy, including adjuvant chemotherapy, which can be tailored to the individual patient's risk of developing recurrence.

ACKNOWLEDGMENT

The authors thank Roderick J. Turner, Edward F. Barroga, and J. Patrick Barron, for their editorial review of the English article.

REFERENCES

1. Goya T, Asamura H, Yoshimura H, et al.; Japanese Joint Committee of Lung Cancer Registry. Prognosis of 6644 resected non-small cell lung cancers in Japan: a Japanese lung cancer registry study. *Lung Cancer* 2005;50:227–234.
2. Asamura H, Goya T, Koshiishi Y, et al.; Japanese Joint Committee of Lung Cancer Registry. A Japanese Lung Cancer Registry study: prognosis of 13,010 resected lung cancers. *J Thorac Oncol* 2008;3:46–52.
3. Sawabata N, Miyaoka E, Asamura H, et al.; Japanese Joint Committee for Lung Cancer Registration. Japanese lung cancer registry study of 11,663 surgical cases in 2004: demographic and prognosis changes over decade. *J Thorac Oncol* 2011;6:1229–1235.
4. Rami-Porta R, Ball D, Crowley J, et al.; International Staging Committee; Cancer Research and Biostatistics; Observers to the Committee; Participating Institutions. The IASLC Lung Cancer Staging Project: proposals for the revision of the T descriptors in the forthcoming (seventh) edition of the TNM classification for lung cancer. *J Thorac Oncol* 2007;2:593–602.
5. Agarwal M, Brahmanday G, Chmielewski GW, Welsh RJ, Ravikrishnan KP. Age, tumor size, type of surgery, and gender predict survival in early stage (stage I and II) non-small cell lung cancer after surgical resection. *Lung Cancer* 2010;68:398–402.
6. Kawai H, Tada A, Kawahara M, et al.; Japan National Hospital Study Group for Lung Cancer. Smoking history before surgery and prognosis in patients with stage IA non-small-cell lung cancer–a multicenter study. *Lung Cancer* 2005;49:63–70.
7. Okada M, Sakamoto T, Nishio W, Uchino K, Tsubota N. Characteristics and prognosis of patients after resection of nonsmall cell lung carcinoma measuring 2 cm or less in greatest dimension. *Cancer* 2003;98:535–541.
8. Ruffini E, Asioli S, Filosso PL, et al. Significance of the presence of microscopic vascular invasion after complete resection of Stage I-II pT1-T2N0 non-small cell lung cancer and its relation with T-Size categories: did the 2009 7th edition of the TNM staging system miss something? *J Thorac Oncol* 2011;6:319–326.
9. Bréchot JM, Chevret S, Charpentier MC, et al. Blood vessel and lymphatic vessel invasion in resected nonsmall cell lung carcinoma. Correlation with TNM stage and disease free and overall survival. *Cancer* 1996;78:2111–2118.
10. Tsuchiya T, Akamine S, Muraoka M, et al. Stage IA non-small cell lung cancer: vessel invasion is a poor prognostic factor and a new target of adjuvant chemotherapy. *Lung Cancer* 2007;56:341–348.
11. Miyoshi K, Moriyama S, Kunitomo T, Nawa S. Prognostic impact of intratumoral vessel invasion in completely resected pathologic stage I non-small cell lung cancer. *J Thorac Cardiovasc Surg* 2009;137:429–434.
12. Shimada Y, Ishii G, Hishida T, Yoshida J, Nishimura M, Nagai K. Extratumoral vascular invasion is a significant prognostic indicator and a predicting factor of distant metastasis in non-small cell lung cancer. *J Thorac Oncol* 2010;5:970–975.
13. Maeda R, Yoshida J, Ishii G, Hishida T, Nishimura M, Nagai K. Prognostic impact of intratumoral vascular invasion in non-small cell lung cancer patients. *Thorax* 2010;65:1092–1098.
14. Ichinose Y, Yano T, Asoh H, Yokoyama H, Yoshino I, Katsuda Y. Prognostic factors obtained by a pathologic examination in completely

resected non-small-cell lung cancer. An analysis in each pathologic stage. *J Thorac Cardiovasc Surg* 1995;110:601–605.
15. Thomas P, Doddoli C, Thirion X, et al. Stage I non-small cell lung cancer: a pragmatic approach to prognosis after complete resection. *Ann Thorac Surg* 2002;73:1065–1070.
16. Maeda R, Yoshida J, Ishii G, Hishida T, Nishimura M, Nagai K. Poor prognostic factors in patients with stage IB non-small cell lung cancer according to the seventh edition TNM classification. *Chest* 2011;139:855–861.
17. Maeda R, Yoshida J, Ishii G, et al. Long-term survival and risk factors for recurrence in stage I non-small cell lung cancer patients with tumors up to 3 cm in maximum dimension. *Chest* 2010;138:357–362.
18. Harada M, Hato T, Horio H. Intratumoral lymphatic vessel involvement is an invasive indicator of completely resected pathologic stage I non-small cell lung cancer. *J Thorac Oncol* 2011;6:48–54.
19. Kobayashi N, Toyooka S, Soh J, et al. Risk factors for recurrence and unfavorable prognosis in patients with stage I non-small cell lung cancer and a tumor diameter of 20 mm or less. *J Thorac Oncol* 2007;2:808–812.
20. Leslie Sobin MG CW (Ed). TNM Classification of Malignant Tumors, 7th Ed. Geneva, UICC International Union Against Cancer, 2009, pp 136–146.
21. William D, Travis EB HKM-H, Curtis C. Harris (Ed). Pathology and Genetics of Tumors of the Lung, Pleura, Thymus and Heart. Lyon, World Health Organization Classification of Tumours, 2004, pp 9–124.
22. Chang MY, Mentzer SJ, Colson YL, et al. Factors predicting poor survival after resection of stage IA non-small cell lung cancer. *J Thorac Cardiovasc Surg* 2007;134:850–856.
23. Sun Z, Aubry MC, Deschamps C, et al. Histologic grade is an independent prognostic factor for survival in non-small cell lung cancer: an analysis of 5018 hospital- and 712 population-based cases. *J Thorac Cardiovasc Surg* 2006;131:1014–1020.
24. Chung CK, Zaino R, Stryker JA, O'Neill M Jr, DeMuth WE Jr. Carcinoma of the lung: evaluation of histological grade and factors influencing prognosis. *Ann Thorac Surg* 1982;33:599–604.
25. Fujisawa T, Yamaguchi Y, Saitoh Y, Hiroshima K, Ohwada H. Blood and lymphatic vessel invasion as prognostic factors for patients with primary resected nonsmall cell carcinoma of the lung with intrapulmonary metastases. *Cancer* 1995;76:2464–2470.
26. Shimizu K, Yoshida J, Nagai K, et al. Visceral pleural invasion is an invasive and aggressive indicator of non-small cell lung cancer. *J Thorac Cardiovasc Surg* 2005;130:160–165.
27. Saijo T, Ishii G, Ochiai A, et al. Evaluation of extratumoral lymphatic permeation in non-small cell lung cancer as a means of predicting outcome. *Lung Cancer* 2007;55:61–66.
28. Winton T, Livingston R, Johnson D, et al.; National Cancer Institute of Canada Clinical Trials Group; National Cancer Institute of the United States Intergroup JBR.10 Trial Investigators; . Vinorelbine plus cisplatin vs. observation in resected non-small-cell lung cancer. *N Engl J Med* 2005;352:2589–2597.
29. Arriagada R, Bergman B, Dunant A, Le Chevalier T, Pignon JP, Vansteenkiste J; International Adjuvant Lung Cancer Trial Collaborative Group. Cisplatin-based adjuvant chemotherapy in patients with completely resected non-small-cell lung cancer. *N Engl J Med* 2004;350:351–360.
30. Douillard JY, Rosell R, De Lena M, et al. Adjuvant vinorelbine plus cisplatin versus observation in patients with completely resected stage IB-IIIA non-small-cell lung cancer (Adjuvant Navelbine International Trialist Association [ANITA]): a randomised controlled trial. *Lancet Oncol* 2006;7:719–727.
31. Kato H, Ichinose Y, Ohta M, et al.; Japan Lung Cancer Research Group on Postsurgical Adjuvant Chemotherapy. A randomized trial of adjuvant chemotherapy with uracil-tegafur for adenocarcinoma of the lung. *N Engl J Med* 2004;350:1713–1721.
32. Hamada C, Tsuboi M, Ohta M, et al. Effect of postoperative adjuvant chemotherapy with tegafur-uracil on survival in patients with stage IA non-small cell lung cancer: an exploratory analysis from a meta-analysis of six randomized controlled trials. *J Thorac Oncol* 2009;4:1511–1516.

Surg Today (2012) 42:899–902
DOI 10.1007/s00595-012-0166-0

CASE REPORT

An intrapericardial foregut cyst: report of a thoracoscopically resected case

Yujin Kudo · Shuji Ichinose · Hiroaki Kataba · Jitsuo Usuda · Naohiro Kajiwara · Tatsuo Ohira · Nobuki Nakamura · Toshitaka Nagao · Norihiko Ikeda

Received: 6 April 2011 / Accepted: 27 July 2011 / Published online: 18 March 2012

Abstract Intrapericardial foregut cysts are rare, and are usually found serendipitously. An abnormal shadow was incidentally found on a chest X-ray film of a 45-year-old asymptomatic female undergoing a regular check-up. Computed tomography revealed a smooth-walled, left mediastinal cyst (70 × 46 mm) immediately adjacent to the pericardium and left ventricle. We performed video-assisted thoracic surgery, which suggested that the lesion had macroscopically originated from the epicardium. However, the resected cyst was histologically determined to be an intrapericardial foregut cyst. This experience taught us that, while intrapericardial cysts possess the latent possibility of causing sudden death, cardiac failure, or eventual malignant changes, carefully planned and meticulously executed resection, avoiding damage to adjacent organs or vessels, is recommended.

Keywords Thoracoscopy · VATS · Mediastinum · Cysts · Pericardium

Introduction

Primary cysts constitute 25 % of all mediastinal masses [1]. Foregut cysts represent an abnormal budding from either the dorsal or ventral portion of the primitive foregut, and 3 types have been described: bronchogenic, intramural esophageal and enteric cysts [2]. They rarely develop within the pericardium and are often asymptomatic and detected only incidentally on chest X-ray examinations. We herein report a very rare case of intrapericardial foregut cyst resected using video-assisted thoracic surgery (VATS).

Y. Kudo (✉) · S. Ichinose · H. Kataba · J. Usuda · N. Kajiwara · T. Ohira · N. Ikeda
Department of Surgery, Tokyo Medical University, 6-7-1 Nishishinjuku, Shinjuku-ku, Tokyo 160-0023, Japan
e-mail: yjnkudo@gmail.com

N. Nakamura · T. Nagao
Department of Anatomic Pathology, Tokyo Medical University, Tokyo, Japan

Case report

A 45-year-old asymptomatic female showed an abnormal shadow on her chest X-ray film at a medical check-up in January 2010, and she was referred to our hospital. Her past history, physical examination, laboratory data, electrocardiography results and pulmonary function tests were unremarkable. The radiographic findings showed a smooth-walled, left mediastinal cyst (70 × 46 mm) immediately adjacent to the pericardium and left ventricle (Figs. 1, 2).

VATS was performed via the left side in the right lateral decubitus position. The camera port was placed at the 6th intercostal space, and the utility ports were inserted at the 3rd and 5th intercostal spaces. When a 30° 10 mm viewing scope was inserted, the mass was not visualized in the left thoracic cavity. VATS revealed the lesion to be located within the pericardium. After opening the pericardium, a large, smooth, slightly red mass was observed. Puncture and aspiration of the cyst yielded 150 cc of an opaque whitish material (Fig. 3a). We examined the cyst wall, which was near the left auricle and left anterior descending coronary artery (LAD), and it was macroscopically thought to originate from the epicardium of the left ventricle (Fig. 3b). Because its extremely close contact with vascular structures precluded complete resection, we used an ultrasonic scalpel to partially resect the cyst. The part of the

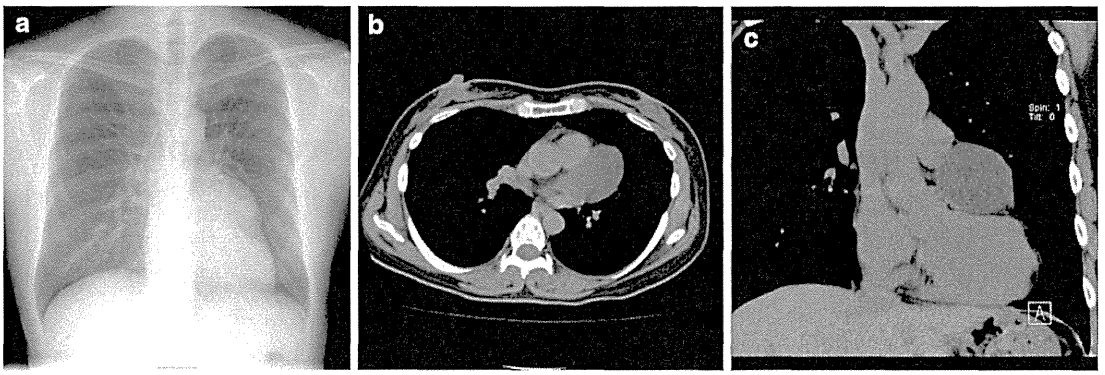

Fig. 1 **a** A chest X-ray film showing a protrusion on the left side of a mediastinal shadow. **b**, **c** Chest computed tomographic images showing a smooth-walled, left mediastinal cyst adjacent to the pericardium and left ventricle

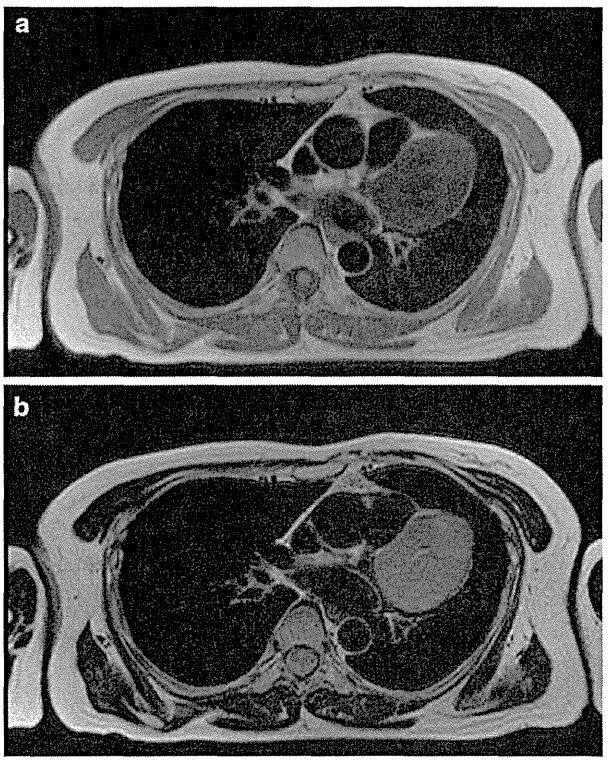

Fig. 2 T1-weighted magnetic resonance images show a low-intensity lesion (**a**), and a T2-weighted image shows a high-intensity lesion (**b**)

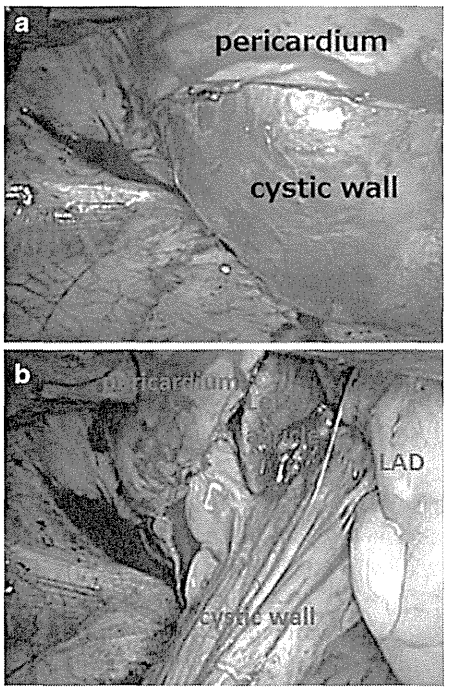

Fig. 3 The thoracoscopic findings. **a** The cyst was exposed after opening the pericardium. **b** The cyst appeared to arise from the epicardium of the left ventricle between the left auricle and the LAD

cystic wall adherent to the left ventricle was not resected to avoid myocardial damage. Since the opened pericardial area was small, and we estimated that there was a low risk of cardiac ectopia, the pericardium was left unsutured to prevent heart compression should the cyst recur.

A histopathological examination of the specimens (50 × 25 × 8 mm, 35 × 15 × 8 mm; divided) revealed that the cystic wall consisted mainly of elastic fibers and hyaline tissues partially covered by a mucinous epithelium, and that it contained smooth muscle (mucin and SMA detected on immunohistochemistry, respectively; MUC6+, MUC1±, MUC5−, MUC2−). There was no evidence of cartilage, seromucinous glands, or neuroectodermal structures such as skin, appendages of skin, or neuronal tissue. The final diagnosis was an intrapericardial foregut cyst (Fig. 4). The cystic fluid was sterile in the cultures for bacteria and fungi. The patient had an uneventful course and was discharged on postoperative day 7. Six months later, CT showed no evidence of recurrence.

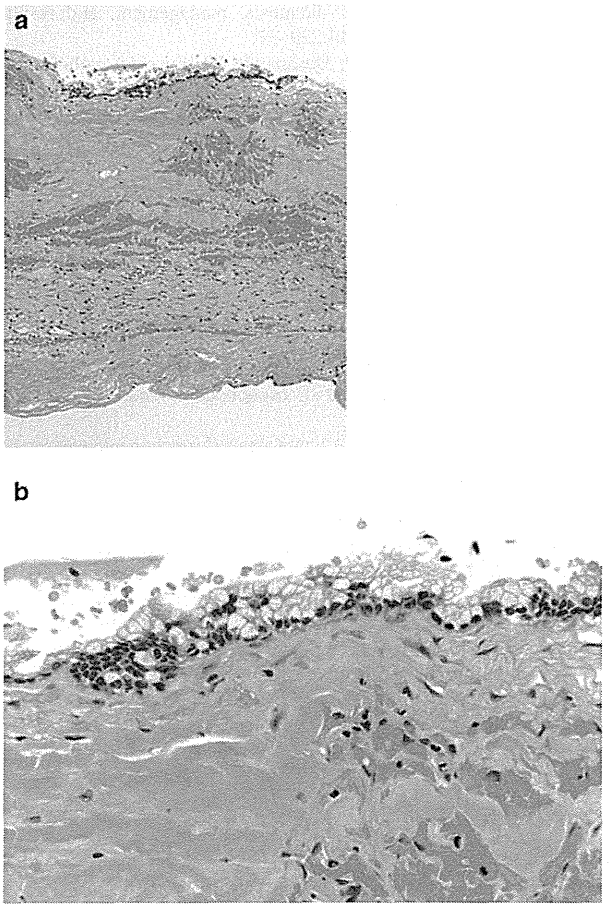

Fig. 4 Histopathologically, H&E staining showed the cyst to be covered with a mucinous epithelium without cilia (**a**), and containing smooth muscle bundles (**b**)

Discussion

Mediastinal cysts are classified based on their anatomic location and histomorphology. Histologically, they can be classified as a foregut cyst, cystic teratoma, thymic cyst, pericardial cyst, or into a large miscellaneous group. Foregut cysts account for approximately 20–50 % of mediastinal cysts, and are categorized on the basis of their anomalous embryonic origin into either bronchogenic, esophageal, gastric or undifferentiated cysts [1, 2]. They typically show abnormal growth from either the dorsal or ventral portion of the primitive foregut.

However, foregut cysts within the pericardium are rare. There have been a limited number of reports on intrapericardial cysts, such as foregut cysts (especially bronchogenic cysts) and pericardial cysts. An intrapericardial cystic mass was first described by Joel [3]. Beck reported the first intrapericardial teratomatous cyst removed surgically [4]. Recently, reports on the successful surgical extirpation of intrapericardial bronchogenic cysts have appeared. Excision has replaced drainage and marsupialization as the therapy of choice for any bronchogenic cyst, regardless of its location.

The differential diagnoses of the present case included pericardial cysts, parasitic cysts and cystic mesotheliomas. During surgery, the cystic wall was in close contact with the epicardium, and the cyst was noted to be filled with an opaque whitish material. Histologically, the cystic wall was mainly lined by mucinous epithelium, but at each extremity of the wall, there were small areas with single layers of flat cells, such as serosal or endothelial cells. Based on these findings, we diagnosed the patient to have a foregut cyst.

Foregut cyst development within the chest can be explained embryologically, but various theories have been postulated regarding its developmental embryological mechanics. The pericardial and pleural cavities communicate with each other until the 4th or 5th week of intrauterine life. Due to the close proximity of the heart and lungs at this development stage, a cyst developing from a lung bud could be encapsulated by the pericardium. The presence of gastrointestinal tract tissues can be explained embryologically, since the lung buds are derived from the pharyngeal part of the foregut [5].

The symptoms of mediastinal cysts are most frequently caused by compression of the affected organ, which leads to coughing, dyspnea, and chest pain, among other symptoms. Several studies have indicated that surgical resection is the treatment of choice for symptomatic or complicated cysts [6, 7]. On the other hand, the management of asymptomatic lesions is controversial, with some authors suggesting only continued observation [6, 8]. Although the complication rate is low, severe and life-threatening circumstances may occur, such as cardiac tamponade from an untreated enteric or bronchogenic cyst of the mediastinum, or due to the rupture of a cyst [9]. Furthermore, malignant transformation of mediastinal foregut cysts may also occur [10]. Resection of an intrapericardial cyst is recommended even in asymptomatic patients, due to its potential for complications and latent malignant changes.

In the present case, we performed a VATS resection of the cyst. First, we used an ultrasonic scalpel when resecting the cystic wall to avoid electrocautery-induced arrhythmia, of which there was no evidence intraoperatively. Second, early cyst decompression improved the mobility and exposure of the posterior aspect. Therefore, we confirmed the positional relationship of the cyst and the left auricle, LAD, and epicardium. However, the extremely close contact of the cyst with important vascular structures precluded safe complete resection, and thus, the cyst was only partially excised. Complete resection is preferable, but surgical difficulties arising from adhesion to adjacent organs or vessels were present, and a small remnant of the cystic wall may remain even after a mucosal lining

resection aimed at preventing recurrence. There are reports of recurrence of bronchogenic cysts after incomplete surgical removal. One important aspect of these recurrences was the time of recurrence (20 and 25 years) after initial surgery. Therefore, all patients undergoing partial resection or needle drainage of bronchogenic cysts should be considered at risk for recurrence for at least 20 to 30 years [11].

In conclusion, we herein described the minimally invasive, successful treatment of an intrapericardial foregut cyst. Since the resection of an intrapericardial foregut cyst is a potentially life-threatening operation, it must be considered carefully and meticulously performed to avoid damage to adjacent organs.

Acknowledgments We are indebted to Mr. R.J. Turner, Assistant Professor; E.F. Barroga and Professor J.P. Barron, Chairman of the Department of International Medical Communications at Tokyo Medical University for their review of the English in the manuscript.

Conflict of interest The authors declare no conflict of interest regarding this study.

References

1. Davis RD Jr, Oldham HN Jr, Sabiston DC Jr. Primary cysts and neoplasms of the mediastinum: recent changes in clinical presentation, methods of diagnosis, management, and results. Ann Thorac Surg. 1987;44:229–37.
2. Petkar M, Vaideeswar P, Deshpande JR. Surgical pathology of cystic lesions of the mediastinum. J Postgrad Med. 2001;47:235–9.
3. Joel VJ. Ein teratoma auf der arteria pulmonalis innerhalb des herzbeutels. Anatomie. 1890;122:381–6.
4. Beck CS. An intrapericardial teratoma and a tumor of the heart: both removed operatively. Ann Surg. 1942;116:161–74.
5. Gomes MN, Hufnagel CA. Intrapericardial bronchogenic cysts. Am J Cardiol. 1975;36:817–22.
6. Sirivella S, Ford WB, Zikria EA, Miller WH, Samadani SR, Sullivan ME. Foregut cysts of the mediastinum. Results in 20 consecutive surgically treated cases. J Thorac Cardiovasc Surg. 1985;90:776–82.
7. Patel SR, Meeker DP, Biscotti CV, Kirby TJ, Rice TW. Presentation and management of bronchogenic cysts in the adult. Chest. 1994;106:79–85.
8. Bolton JW, Shahian DM. Asymptomatic bronchogenic cysts: what is the best management? Ann Thorac Surg. 1992;53:1134–7.
9. Iglesias Sentis M, Belda Sanchis J, Gimferrer Garolera JM, Catalan Biela M, Rubio Garay M, Ramirez Ruz J. Mediastinal enteric cyst: unusual clinical presentation and histopathology. Arch Bronconeumol. 2004;40:185–7.
10. Olsen JB, Clemmensen O, Andersen K. Adenocarcinoma arising in a foregut cyst of the mediastinum. Ann Thorac Surg. 1991;51:497–9.
11. Read CA, Moront M, Carangelo R, Holt RW, Richardson M. Recurrent bronchogenic cyst. An argument for complete surgical excision. Arch Surg. 1991;126:1306–8.

European Journal of Radiology 81 (2012) 2877–2886

Contents lists available at SciVerse ScienceDirect

European Journal of Radiology

journal homepage: www.elsevier.com/locate/ejrad

Pulmonary nodules: Effect of adaptive statistical iterative reconstruction (ASIR) technique on performance of a computer-aided detection (CAD) system—Comparison of performance between different-dose CT scans

Masahiro Yanagawa*, Osamu Honda, Ayano Kikuyama, Tomoko Gyobu, Hiromitsu Sumikawa, Mitsuhiro Koyama, Noriyuki Tomiyama

Department of Radiology, Osaka University Graduate School of Medicine, 2-2 Yamadaoka, Suita-city, Osaka 565-0871, Japan

ARTICLE INFO

Article history:
Received 25 February 2011
Received in revised form 30 August 2011
Accepted 1 September 2011

Keywords:
Chest CT
Adaptive statistical iterative reconstruction (ASIR)
Computer-aided detection (CAD)
Radiation dose

ABSTRACT

Purpose: To evaluate the effects of ASIR on CAD system of pulmonary nodules using clinical routine-dose CT and lower-dose CT.

Materials and methods: Thirty-five patients (body mass index, $22.17 \pm 4.37\,kg/m^2$) were scanned by multidetector-row CT with tube currents (clinical routine-dose CT, automatically adjusted mA; lower-dose CT, 10 mA) and X-ray voltage (120 kVp). Each 0.625-mm-thick image was reconstructed at 0%-, 50%-, and 100%-ASIR: 0%-ASIR is reconstructed using only the filtered back-projection algorithm (FBP), while 100%-ASIR is reconstructed using the maximum ASIR and 50%-ASIR implies a blending of 50% FBP and ASIR. CAD output was compared retrospectively with the results of the reference standard which was established using a consensus panel of three radiologists. Data were analyzed using Bonferroni/Dunn's method. Radiation dose was calculated by multiplying dose-length product by conversion coefficient of 0.021.

Results: The consensus panel found 265 non-calcified nodules ≤30 mm (ground-glass opacity [GGO], 103; part-solid, 34; and solid, 128). CAD sensitivity was significantly higher at 100%-ASIR [clinical routine-dose CT, 71% (overall), 49% (GGO); lower-dose CT, 52% (overall), 67% (solid)] than at 0%-ASIR [clinical routine-dose CT, 54% (overall), 25% (GGO); lower-dose CT, 36% (overall), 50% (solid)] ($p < 0.001$). Mean number of false-positive findings per examination was significantly higher at 100%-ASIR (clinical routine-dose CT, 8.5; lower-dose CT, 6.2) than at 0%-ASIR (clinical routine-dose CT, 4.6; lower-dose CT, 3.5; $p < 0.001$). Effective doses were 10.77 ± 3.41 mSv in clinical routine-dose CT and 2.67 ± 0.17 mSv in lower-dose CT.

Conclusion: CAD sensitivity at 100%-ASIR on lower-dose CT is almost equal to that at 0%-ASIR on clinical routine-dose CT. ASIR can increase CAD sensitivity despite increased false-positive findings.

1. Introduction

In the field of computed tomography (CT), multi-detector row CT (MDCT) units equipped with garnet detectors have recently become available. The most advantageous feature of MDCT with garnet detectors is the improved spatial resolution (high-definition imaging at up to 230-μm resolution), allowing peripheral thin or fine linear opacities such as bronchioles to be visualized clearly in transverse CT images [1].

The reconstruction algorithm is another important factor affecting image quality. Adaptive statistical iterative reconstruction (ASIR) is a recently developed reconstruction algorithm applicable to MDCT with garnet detectors based on the iterative reconstruction algorithm. Iterative reconstruction is already used for image reconstruction in positron-emission tomography (PET) and single photon emission CT (SPECT), using an algorithm to correct image data with an assortment of models [2]. ASIR was developed using only one corrective model to address image noise. This technique is used to solve one of the primary problems of dose reduction for CT with the conventional filtered back-projection algorithm. ASIR can make adjustments for fluctuations in projection measurement due to limited photon statistics and electronic noise while taking into account statistical modeling of the reconstructed object to balance substantial fluctuations in individual image voxels [3,4]. The

* Corresponding author. Tel.: +81 6 879 3434; fax: +81 6 879 3439.
E-mail addresses: m-yanagawa@radiol.med.osaka-u.ac.jp (M. Yanagawa), ohonda@radiol.med.osaka-u.ac.jp (O. Honda), a-kikuyama@radiol.med.osaka-u.ac.jp (A. Kikuyama), t-gyobu@radiol.med.osaka-u.ac.jp (T. Gyobu), h-sumikawa@radiol.med.osaka-u.ac.jp (H. Sumikawa), m-koyama@radiol.med.osaka-u.ac.jp (M. Koyama), tomiyama@radiol.med.osaka-u.ac.jp (N. Tomiyama).

0720-048X/$ – see front matter © 2011 Elsevier Ireland Ltd. All rights reserved.
doi:10.1016/j.ejrad.2011.09.011

ASIR algorithm enables a time-efficient reduction in pixel variance that is statistically unlikely to be representative of anatomical features, with essentially no trade-off in spatial resolution [5]. ASIR is useful for reducing the dose of CT radiation to the chest and for improving image quality compared with the conventional filtered back-projection algorithm [6–8].

MDCT with garnet detectors can thus improve spatial resolution on chest CT. In addition, ASIR can improve image quality by decreasing image noise on chest CT. We hypothesized that high image quality due to MDCT with garnet detectors and ASIR might influence the performance of computer-aided detection (CAD) systems in detecting pulmonary nodules. However, to the best of our knowledge, no previous studies have evaluated the performance of CAD systems in chest CT imaging using ASIR. The purpose of this study was to evaluate the effects of ASIR on the CAD system of pulmonary nodules using clinical routine- and lower-dose CT.

2. Materials and methods

2.1. Patients

We obtained approval for this prospective clinical study from our internal ethics review board. The study population consisted of consecutive patients with existing or clinically suspicious pulmonary nodules. Subjects comprised 35 patients (18 men, 17 women) with a mean (±standard deviation) age of 64.6 ± 14.6 years (range, 25–90 years). Height (cm), weight (kg), and body mass indices (kg/m^2) were as follows: 157.96 ± 6.56 cm (range, 140–172 cm), 55.66 ± 12.21 kg (range, 27–77 kg), and 22.17 ± 4.37 kg/m^2 (range, 13.7–35.4 kg/m^2). All patients provided informed consent for simultaneous acquisition of chest CT data at both clinical routine-dose (120 kVp, automatically adjusted tube current) and lower-dose (120 kVp, 100 mA) on a 64-channel MDCT (64-MDCT) scanner (GE Discovery CT 750 HD; GE Healthcare, Milwaukee, WI) between June 2009 and September 2009.

2.2. Scanning protocols

The protocol for this 64-MDCT scanner was as follows: detector collimation, 0.625 mm; detector pitch, 0.984; gantry rotation period, 0.4 s; matrix size, 512 × 512 pixels; field of view, 34.5 cm; X-ray voltage, 120 kVp; tube current, automatic exposure control technique with weight-based adjustment for our clinical routine-dose and 100 mA for lower dose; and scan mode, high-resolution mode with 2496 views/rotation. High-resolution mode is a scan mode applicable only to garnet-based CT with the optical characteristics of a garnet gemstone scintillator. The number of views per rotation in high-resolution mode, which is 2.53-times as many as in normal mode with 984 views/rotation, provides detailed tissue information by increasing in-plane resolution in the x–y plane of scanning.

2.3. Images using ASIR technique

First, axial thin-section CT images, 0.625 mm thick, were reconstructed using a high-definition bone (HD-bone) reconstruction kernel, and then, using 3 different levels of ASIR (0%, 50%, and 100%). Iterative reconstruction-assisted HD-bone kernel has the potential to improve CT imaging [3]. The 0%-ASIR is the non-ASIR image reconstructed using only the conventional filtered back-projection algorithm, while 100%-ASIR is the reconstructed image using the maximum degree of ASIR and 50%-ASIR implies a blending of 50% filtered back-projection and 50% statistical iterative reconstruction image data.

2.4. CAD system

CT images were transferred to workstations (Advantage Workstation 4.2; GE Healthcare) and a Lung VCAR software (GE Healthcare: http://www.gehealthcare.com/aw/applications/lung-vcar) was used as the CAD system [9]. This software can segment pulmonary nodules with ground-glass opacity (GGO). Solid nodules are segmented using watershed-based segmentation. For nodules classified as part-solid, the segmentation algorithm initially works for the solid component using the algorithm for solid nodule segmentation. In a parallel process, the non-solid portion of the region is segmented using an adaptive-threshold-based method. For nodules classified as non-solid, the application performs adaptive-threshold-based segmentation followed by morphological pruning.

2.5. Reference standard

To determine the reference standard, two independent chest radiologists (with 9 and 18 years of experience) read the entire set of images from 0%-ASIR on clinical routine-dose CT and evaluated them on a 5-megapixel, 21-in. monochrome LCD monitor without prior knowledge of clinical information. Images were initially displayed with a window level of −700 HU and a window width of 1200 HU, but the radiologists were free to alter these values at their discretion. The maximum diameter of each nodule was measured using calipers on the monitor and was recorded. Each radiologist independently recorded all non-calcified pulmonary nodules with a diameter ≤30 mm on CT scans using a procedure similar to that used in routine clinical practice. The location of pulmonary nodules was classified into three groups. We evenly divided the lung field into three areas: peripheral (on the side of chest wall); middle; and central (on the side of lung hilum). Pulmonary nodules were classified into three categories based on the internal density of the nodule: solid nodule; localized GGO; and part-solid nodule. Solid nodules are characterized by high contrast on CT, localized GGO is characterized by a hazy increase in lung attenuation that does not obscure the underlying vascular markings [10], and part-solid nodules exhibit the characteristics of both solid nodules and localized GGO. Ultimately, candidate lesions were classified as true-positive or false-positive findings by a consensus panel, which included the same two radiologists (9 and 18 years of experience) and an adjudicator (with 16 years of experience) as needed.

2.6. Criterion for evaluating findings detected by the CAD system

The output of the CAD system was only assessed retrospectively, in comparison with the results of the reference standard. If the segmented area of a nodule detected by the CAD system overlapped with or was almost in contact with the delineated area of a nodule identified by radiologists, the nodule was considered to be a detected one; otherwise, the nodule was considered to have been missed by the CAD system and was classified as false-positive findings.

2.7. Radiation dose assessment

To assess the radiation dose associated with chest CT, we recorded the volume CT dose index (CTDIvol) and the total dose-length product (DLP), which represents the total absorbed dose for all scan series acquired in our CT protocol. Effective doses were estimated from the total DLP using a coefficient of 0.021 in accordance with International Commission on Radiological Protection (ICRP) Publication 103 [11].

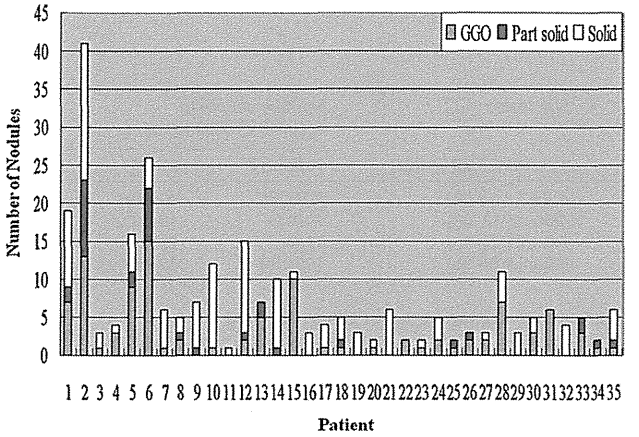

Fig. 1. The distribution of 265 non-calcified nodules with 103 GGO, 34 part-solid, and 128 solid across the 35 patients is shown. GGO, ground-glass opacity.

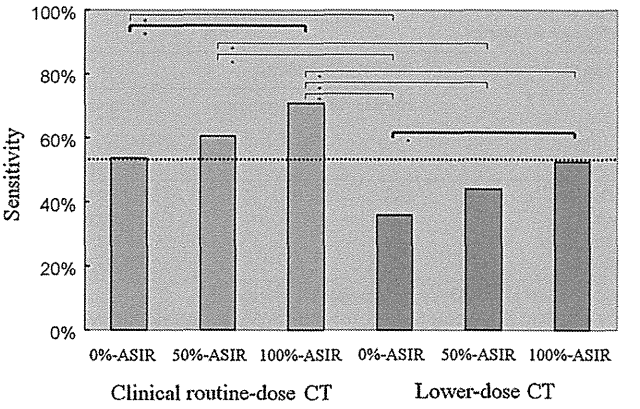

Fig. 2. Graph of the sensitivity of overall nodules for CAD at different levels of ASIR on both clinical routine-dose CT and lower-dose CT (blue bars, clinical routine-dose CT; and red bars, lower-dose CT). Clinical routine-dose CT: 0%-ASIR (54%), 50%-ASIR (61%), and 100%-ASIR (71%). Lower-dose CT: 0%-ASIR (36%), 50%-ASIR (44%), and 100%-ASIR (52%). Sensitivity at 0%-ASIR on clinical routine-dose CT is almost equal to that at 100%-ASIR on lower-dose CT (dotted line). CAD, computer-aided detection; ASIR, adaptive statistical iterative reconstruction. *$p < 0.001$ significant differences using analysis of variance (ANOVA, Bonferroni/Dunn's method). Bold arcs show the significant difference between 0%- and 100%-ASIR.

2.8. Statistical analysis

All statistical analyses were performed using commercially available software (StatView version 5.0; SAS Institute, Cary, NC, USA). Data were analyzed using analysis of variance (ANOVA) with post hoc testing using Bonferroni/Dunn's method for multiple comparisons. All data consisted of the sensitivity of nodules according to the three radiological patterns, the sensitivity of nodules according to nodule size, and the mean number of false-positive findings per scan on clinical routine- and lower-dose CT images (0%-ASIR, 50%-ASIR, and 100%-ASIR, respectively). A p value <0.05 was considered significant.

3. Results

3.1. Results of reference standard

The consensus panel found 265 non-calcified nodules in 35 patients, with 103 GGO, 34 part-solid, and 128 solid. The number of nodules per patient, mean diameter of each nodule, and number of nodules according to location are summarized in Table 1. The distribution of all nodules across the 35 patients is shown in Fig. 1.

3.2. Results of CAD according to the three radiological patterns

Sensitivity data for the detection of each nodule with the three radiological patterns and the number of false-positive findings per scan for the CAD on clinical routine- and lower-dose CT are shown in Table 2. Information on false-positive findings for the CAD system is summarized in Table 3.

With regard to overall nodules, sensitivity of the CAD tended to increase with increasing degree of ASIR on both clinical routine- and lower-dose CT (Fig. 2). In particular, sensitivity was significantly higher at 100%-ASIR (clinical routine-dose, 71%; lower-dose, 52%) than at 0%-ASIR (clinical routine-dose, 54%; lower-dose, 36%; $p < 0.001$). Comparing clinical routine-dose CT with lower-dose CT, sensitivity was significantly higher at 0%-ASIR on clinical routine-dose CT than at 0%-ASIR on lower-dose CT ($p < 0.001$). Sensitivity at 50%-ASIR on clinical routine-dose CT was significantly higher than that at 0%- or 50%-ASIR on lower-dose CT ($p < 0.001$). Sensitivity at 100%-ASIR on clinical routine-dose CT was significantly higher than that at 0%-, 50%-, or 100%-ASIR on lower-dose CT ($p < 0.001$). Sensitivity at 0%-ASIR (54%) on clinical routine-dose CT was almost equal to that at 100%-ASIR (52%) on lower-dose CT (Fig. 2).

With regard to GGO (Fig. 3), sensitivity of the CAD tended to increase with increasing degree of ASIR on both clinical routine- and lower-dose CT. In particular, sensitivity was significantly higher at 100%-ASIR (49%) on clinical routine-dose CT than at 0%-ASIR (25%) on clinical routine-dose CT ($p < 0.001$). Comparing clinical routine- and lower-dose CT, sensitivity was significantly higher at 50%-ASIR on clinical routine-dose CT than at 0%-ASIR on lower-dose CT ($p < 0.001$). Sensitivity was significantly higher at 100%-ASIR on clinical routine-dose CT than at 0%-, 50%-, or 100%-ASIR on lower-dose CT ($p < 0.001$). Sensitivity at 0%-ASIR (25%) on clinical routine-dose CT was equal to that at 100%-ASIR (25%) on lower-dose CT.

With regard to part-solid nodules (Fig. 4), sensitivity for the CAD tended to be equal or to increase with increasing degree of ASIR on both clinical routine- and lower-dose CT. Comparing clinical routine-dose CT with lower-dose CT, sensitivity was significantly higher at 100%-ASIR on clinical routine-dose CT than at 0%-ASIR on lower-dose CT ($p < 0.001$). Sensitivity at 100%-ASIR on lower-dose CT (79%) was almost equal to that at 0%-ASIR on clinical routine-dose CT (76%).

With regard to solid nodules (Fig. 5), sensitivity for the CAD tended to increase with increasing degree of ASIR on both clinical routine- and lower-dose CT. In particular, sensitivity was significantly higher at 100%-ASIR (67%) on lower-dose CT than at 0%-ASIR (50%; $p < 0.001$). Comparing clinical routine- and lower-dose CT, the results were the same as those for all nodules. Sensitivity at 0%-ASIR (70%) on clinical routine-dose CT was almost equal to that at 100%-ASIR (67%) on lower-dose CT.

False-positive findings for the CAD mainly consisted of peripheral vessels, central vessels, pleural thickening, and mucoid impaction of the bronchus. On clinical routine-dose CT, the mean number of false-positive findings per scan increased significantly with increasing degree of ASIR ($p < 0.001$). On lower-dose CT, the mean number of false-positive findings per scan tended to increase with increasing degree of ASIR. In particular, the mean number of false-positive findings per scan was significantly higher at 100%-ASIR than at 0%-ASIR ($p < 0.001$) (Fig. 6). Comparing clinical routine-dose CT with lower-dose CT, the mean number of false-positive findings per scan at 100%-ASIR on clinical routine-dose CT was significantly higher than that at 0%-, 50%-, or 100%-ASIR on lower-dose CT ($p < 0.001$). The mean number of false-positive

Table 1
Reference standard.

Pattern of nodule	Reference standard					
	Number in all 35 patients	Number per patient	Size (mm)	Number of nodule According to the location		
		Mean number ± SD (range)	Mean size ± SD (range)	Peripheral	Middle	Central
Overall	265	7.4 ± 7.9 (1–41)	4.4 ± 3.2 (2–30)	201/265	42/265	22/265
GGO	103	2.9 ± 3.8 (0–15)	4.5 ± 2.9 (2–24)	74/103	19/103	10/103
Part solid	34	0.9 ± 2.0 (0–10)	5.8 ± 3.0 (2–15)	22/34	8/34	4/34
Solid	128	3.5 ± 3.9 (0–18)	3.9 ± 3.3 (2–30)	105/128	15/128	8/128

GGO, ground-glass opacity; SD, standard deviation.
The lung field was evenly divided into three areas: peripheral (on the side of chest wall), middle, and central (on the side of hilum of the lung).

Table 2
Sensitivity data for the detection of each nodule with three radiologic patterns and number of false-positive findings per scan on clinical routine- and lower-dose CT.

	Sensitivity (%)				Number of false-positive findings	
	Overall	GGO	Part-solid	Solid	Mean per scan	Range per scan
Clinical routine dose						
(a) 0%-ASIR	54	25	76	70	4.6	1–11
(b) 50%-ASIR	61	31	76	80	6.9	1–17
(c) 100%-ASIR	71	49	85	84	8.5	5–21
Lower dose						
(d) 0%-ASIR	36	13	53	50	3.5	1–6
(e) 50%-ASIR	44	17	65	60	4.7	1–9
(f) 100%-ASIR	52	25	79	67	6.2	2–12
*Differences between each group						
(a)–(b)	NS	NS	NS	NS	$p < 0.001$	
(a)–(c)	$p < 0.001$	$p < 0.001$	NS	NS	$p < 0.001$	
(a)–(d)	$p < 0.001$	NS	NS	$p < 0.001$	NS	
(a)–(e)	NS	NS	NS	NS	NS	
(a)–(f)	NS	NS	NS	NS	NS	
(b)–(c)	NS	NS	NS	NS	$p < 0.001$	
(b)–(d)	$p < 0.001$	$p < 0.001$	NS	$p < 0.001$	$p < 0.001$	
(b)–(e)	$p < 0.001$	NS	NS	$p < 0.001$	$p < 0.001$	
(b)–(f)	NS	NS	NS	NS	NS	
(c)–(d)	$p < 0.001$	$p < 0.001$	$p < 0.001$	$p < 0.001$	$p < 0.001$	
(c)–(e)	$p < 0.001$	$p < 0.001$	NS	$p < 0.001$	$p < 0.001$	
(c)–(f)	$p < 0.001$	$p < 0.001$	NS	$p < 0.001$	$p < 0.001$	
(d)–(e)	NS	NS	NS	NS	NS	
(d)–(f)	$p < 0.001$	NS	NS	$p < 0.001$	$p < 0.001$	
(e)–(f)	NS	NS	NS	NS	NS	

GGO, ground-glass opacity; ASIR, adaptive statistical iterative reconstruction; NS, not significant.
* Data were analyzed using analysis of variance (ANOVA, Bonferroni/Dunn's method). A p value of less than 0.05 was considered significant.

Table 3
False-positive findings detected by the CAD system on clinical routine- and lower-dose CT.

	Pattern of false-positive findings	Number of false-positive findings According to the location		
		Peripheral	Middle	Central
Clinical routine dose				
0%-ASIR	Pleural changes (small pleural thickening and inflammatory changes)	39	6	25
	Vessels	20	9	59
	Mucoid impaction	5	0	0
50%-ASIR	Pleural changes (small pleural thickening and inflammatory changes)	41	15	38
	Vessels	28	12	101
	Mucoid impaction	5	1	0
100%-ASIR	Pleural changes (small pleural thickening and inflammatory changes)	63	7	39
	Vessels	31	12	140
	Mucoid impaction	6	0	0
Lower dose				
0%-ASIR	Pleural changes (small pleural thickening and inflammatory changes)	33	4	23
	Vessels	16	3	39
	Mucoid impaction	4	0	0
50%-ASIR	Pleural changes (small pleural thickening and inflammatory changes)	40	7	28
	Vessels	22	4	60
	Mucoid impaction	4	0	0
100%-ASIR	Pleural changes (small pleural thickening and inflammatory changes)	44	8	33
	Vessels	26	7	94
	Mucoid impaction	4	1	0

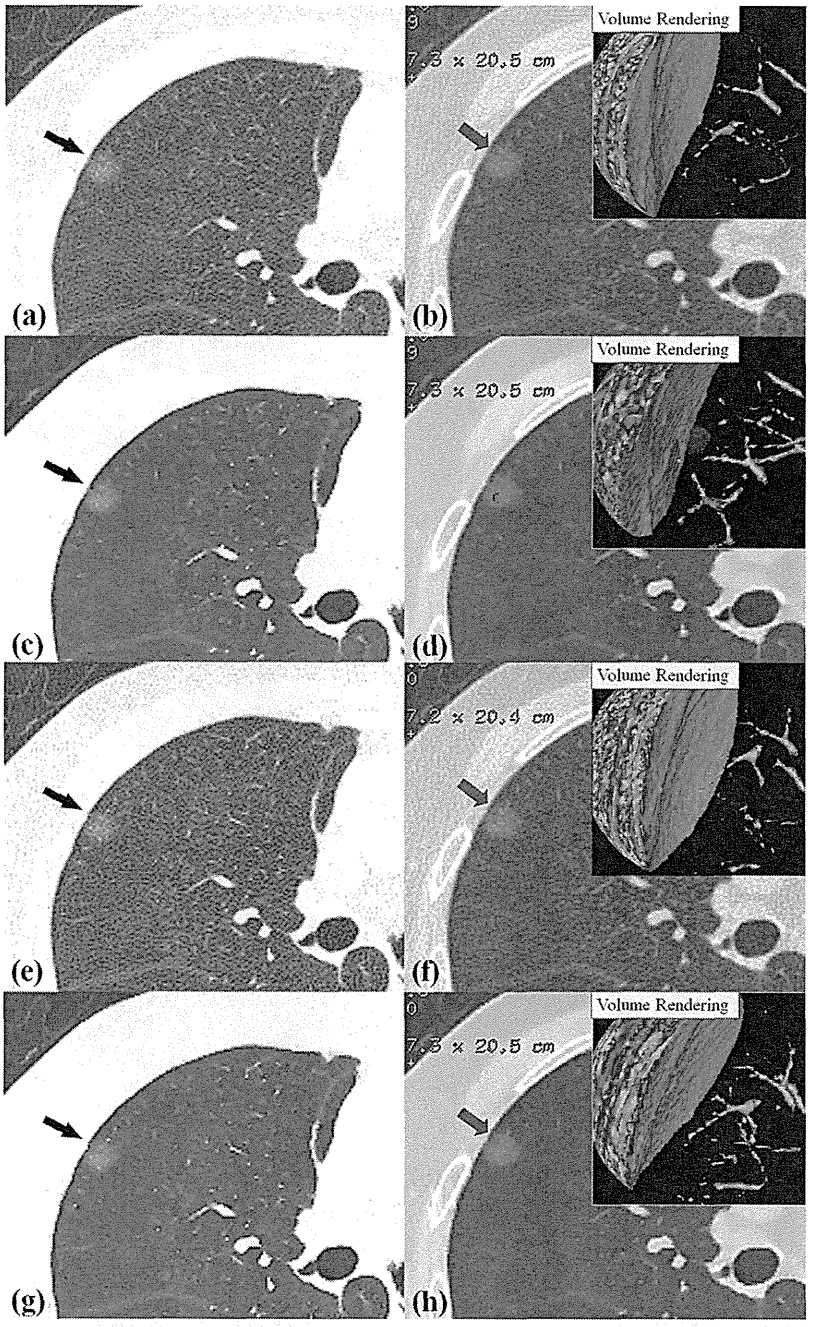

Fig. 3. A case with a ground-glass opacity in a 79-year-old woman. Clinical routine-dose images with 0.625-mm section thickness at (a) 0%-ASIR without CAD (reference standard), (b) 0%-ASIR with CAD, (c) 100%-ASIR without CAD, and (d) 100%-ASIR with CAD. Lower-dose CT images with 0.625-mm section thickness at (e) 0%-ASIR without CAD, (f) 0%-ASIR with CAD, (g) 100%-ASIR without CAD, and (h) 100%-ASIR with CAD. Transverse thin-section CT images with 0.625 mm-thickness show a 10 mm-diameter ground-glass opacity in the peripheral zone of the right upper lobe [black arrows in (a), (c), (e), and (g)]. The CAD system cannot detect this ground-glass opacity on transverse and volume rendering images [blue arrows in (b), (f), and (h)]. Red marks indicate this ground-glass opacity detected by the CAD system on transverse and volume rendering images (d). CAD, computer-aided detection; ASIR, adaptive statistical iterative reconstruction.

findings per scan was significantly higher at clinical routine-dose 50%-ASIR than at lower-dose 0%- or 50%-ASIR ($p < 0.001$).

3.3. Results of CAD according to nodule size

Sensitivity of the CAD according to nodule size tended to be equal or to increase with increasing degree of ASIR on both clinical routine- and lower-dose CT (Table 4). In nodules with diameter $\leq$5 mm ($n = 213$), sensitivity was significantly higher at 100%-ASIR (clinical routine-dose, 66%; lower-dose, 46%) than at 0%-ASIR (clinical routine-dose, 49%; lower-dose, 31%; $p < 0.001$) (Fig. 7(1)). However, in nodules with diameter $\geq$6 mm ($n = 52$), there were significant differences only in sensitivity between clinical routine-dose 100%-ASIR and lower-dose 0%- or 50%-ASIR ($p < 0.001$) (Fig. 7(2)).

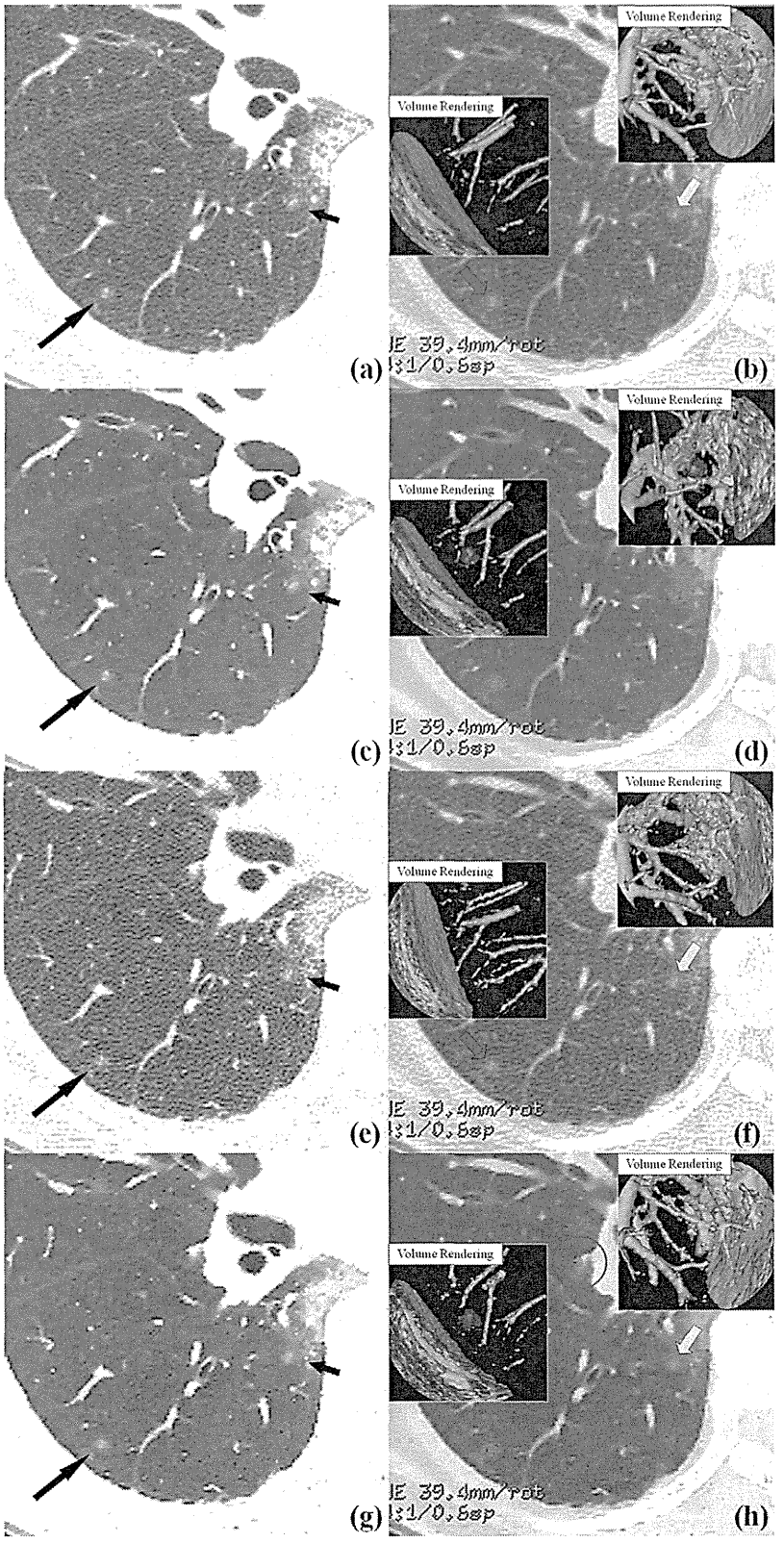

Fig. 4. A case with part-solid nodules in a 64-year-old woman. Clinical routine-dose images with 0.625-mm section thickness at (a) 0%-ASIR without CAD (reference standard), (b) 0%-ASIR with CAD, (c) 100%-ASIR without CAD, and (d) 100%-ASIR with CAD. Lower-dose CT images with 0.625-mm section thickness at (e) 0%-ASIR without CAD, (f) 0%-ASIR with CAD, (g) 100%-ASIR without CAD, and (h) 100%-ASIR with CAD. Transverse thin-section CT images with 0.625 mm-thickness show 4 mm-diameter part-solid nodules in the peripheral zone (long arrows) and the central zone (short arrows) of the right lower lobe in (a), (c), (e), and (g). The CAD system cannot detect the part-solid nodule in the peripheral zone on transverse and volume rendering images [blue arrows in (b) and (f)]. Red marks indicate the part-solid nodule in the peripheral zone detected by the CAD system on transverse and volume rendering images [(d) and (h)]: however, in (h), a red mark in a blue circle indicates a false-positive finding (i.e., vessel) detected

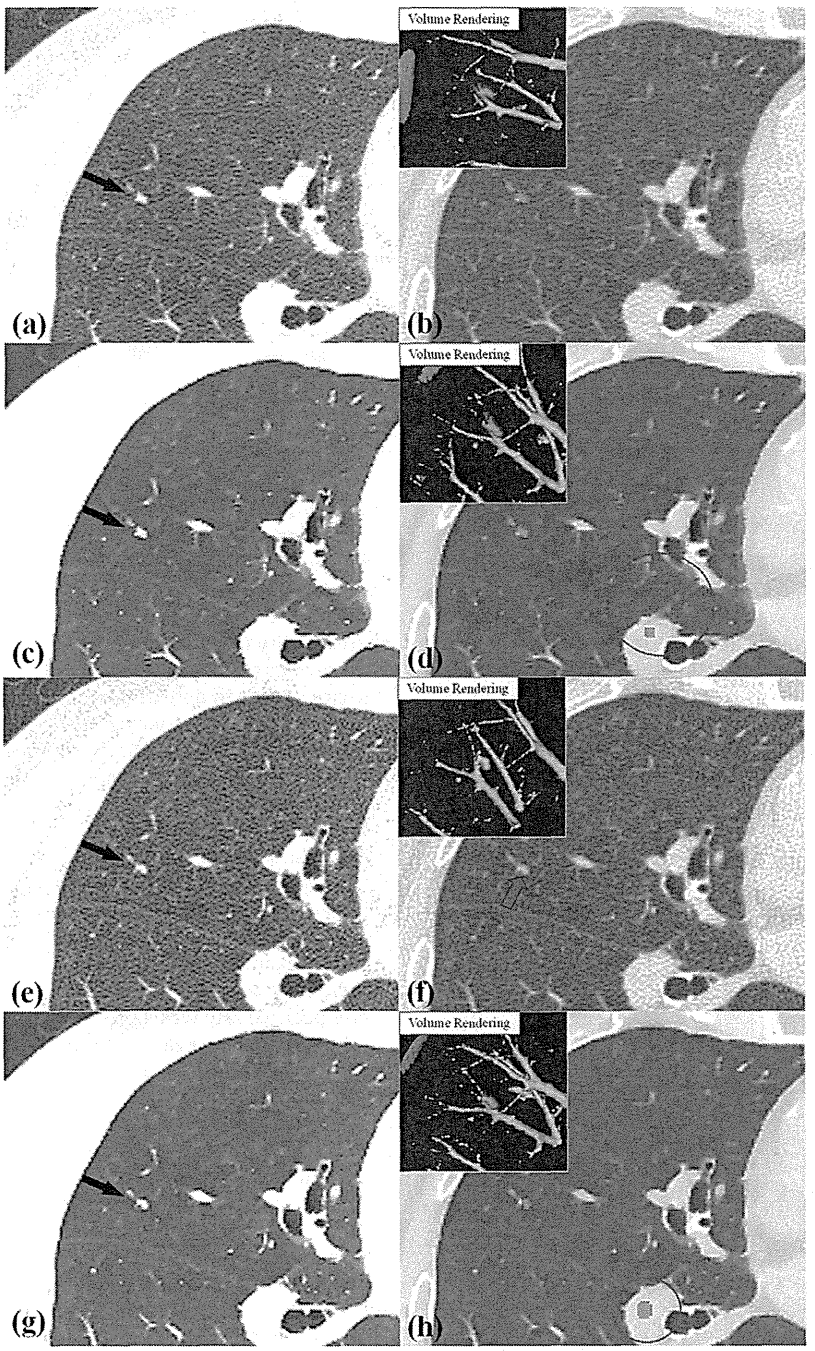

Fig. 5. A case with a solid nodule in a 79-year-old woman. Clinical routine-dose images with 0.625-mm section thickness at (a) 0%-ASIR without CAD (reference standard), (b) 0%-ASIR with CAD, (c) 100%-ASIR without CAD, and (d) 100%-ASIR with CAD. Lower-dose CT images with 0.625-mm section thickness at (e) 0%-ASIR without CAD, (f) 0%-ASIR with CAD, (g) 100%-ASIR without CAD, and (h) 100%-ASIR with CAD. Transverse thin-section CT images with 0.625 mm-thickness show 3 mm-diameter solid nodule in the peripheral zone of the right middle lobe in (a), (c), (e), and (g) (black arrows). The CAD system cannot detect this solid nodule on transverse and volume rendering images only in (f) (a blue arrow). Red marks indicate this solid nodule detected by the CAD system on transverse and volume rendering images [(b), (d), and (h)]: however, in (d) and (h), red marks in blue circles indicate false-positive findings (i.e., vessels) detected by the CAD system. CAD, computer-aided detection; ASIR, adaptive statistical iterative reconstruction.

by the CAD system. The CAD system cannot detect the part-solid nodule in the central zone on transverse and volume rendering images [yellow arrows in (b), (f), and (h)]. Red marks indicate the part-solid nodule in the central zone detected by the CAD system on transverse and volume rendering images (d). CAD, computer-aided detection; ASIR, adaptive statistical iterative reconstruction.

Table 4
Sensitivity data for the detection of each nodule according to nodule size on clinical routine- and lower-dose CT.

Size (mm)	Reference standard (number)	Sensitivity of the CAD system (%)					
		Clinical routine-dose CT			Lower-dose CT		
		0%-ASIR	50%-ASIR	100%-ASIR	0%-ASIR	50%-ASIR	100%-ASIR
2.0–2.9	58	36	48	53	17	28	36
3.0–3.9	78	51	59	64	26	37	44
4.0–4.9	48	52	56	75	46	48	52
5.0–5.9	29	66	76	83	52	62	66
6.0–6.9	12	58	58	75	33	42	58
7.0–7.9	11	91	91	100	64	64	91
8.0–8.9	11	55	64	82	45	45	73
9.0–9.9	3	67	67	67	67	67	67
10.0–10.9	4	75	75	100	75	75	75
11.0–11.9	3	67	67	100	67	67	100
12.0–30.0	8	88	88	100	63	75	88
Total	265	54	61	71	36	44	52

3.4. Results of radiation dose

On clinical routine-dose CT, mean CTDIvol was 14.56 ± 4.67 mGy, mean DLP was 513.07 ± 162.55 mGy cm, and mean estimated effective dose was 10.77 ± 3.41 mSv. On lower-dose CT, mean CTDIvol was 3.48 ± 0.00 mGy, mean DLP was 127.33 ± 8.28 mGy cm, and mean estimated effective dose was 2.67 ± 0.17 mSv.

4. Discussion

The high temporal resolution of MDCT has reduced motion artifacts [12] and the acquisition of images with thin-slice thickness using MDCT has improved the depiction of small pulmonary nodules [13]. The recent garnet-based-detector CT has also significantly improved the quality of lung images [1]. The advent of ASIR for CT has provided improved image quality even with lower-dose CT [3–8]. Therefore, numerous normal and abnormal CT findings including small pulmonary nodules will thus be clearly seen even on lower-dose CT. Although this is exceptional, the number of pulmonary nodules that radiologists will need to identify and may end up inadvertently overlooking is predicted to increase. As previously reported [14–17], CAD is useful for detecting pulmonary nodules efficiently on CT. Understanding the CAD performance on recent MDCT images is very important, along with how ASIR affects detectability using the CAD.

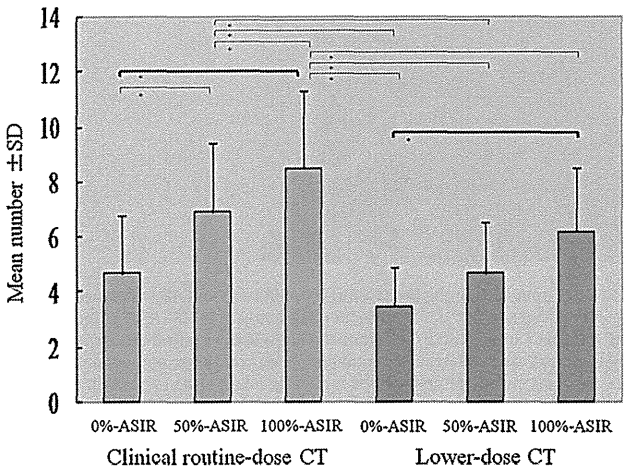

Fig. 6. Graph of the mean number of false-positive findings per scan at different levels of ASIR on both clinical routine- and lower-dose CT (blue bars, clinical routine-dose CT; and red bars, lower-dose CT). Clinical routine-dose CT (mean number ± SD): 0%-ASIR (4.6 ± 2.1), 50%-ASIR (6.9 ± 2.5), and 100%-ASIR (8.5 ± 2.8). Lower-dose CT (mean number ± SD): 0%-ASIR (3.5 ± 1.4), 50%-ASIR (4.7 ± 1.8), and 100%-ASIR (6.2 ± 2.3). SD, standard deviation; ASIR, adaptive statistical iterative reconstruction. *$p < 0.001$ significant differences using analysis of variance (ANOVA, Bonferroni/Dunn's method). Bold arcs show the significant difference between 0%- and 100%-ASIR.

Previous studies of CAD without ASIR have revealed that the sensitivity of CAD in detecting lung nodules is highly variable among studies; these values vary depending on several conditions, such as the type of CAD system used, variations in the characteristics of the nodules examined, and the acquisition criteria. For instance, the sensitivity of other CAD systems for solid nodules applied to MDCT with sections 0.625–1.5 mm thick varies from 16.5% to 86% with false-positive rates of approximately 0.95–10.9/examination [17–20]. The sensitivity of the same CAD system (i.e., lung VCAR) applied to MDCT with sections 0.625 mm thick was as follows: 21% for GGO, 48% for part-solid, and 58% for solid [9]. False-positive rate was 5.7/examination [9]. In the present study, the CAD sensitivity for GGO, part-solid, and solid was 25%, 76%, and 70%, respectively. False positive rate was 4.6/examination.

In the present evaluation of clinical routine-dose CT images, sensitivity of CAD for overall nodules tended to increase with increasing degree of ASIR. Sensitivity was significantly higher at 100%-ASIR than at 0%-ASIR. In particular, using 100%-ASIR significantly improved the sensitivity of fine nodules such as GGO and small nodules with a diameter ≤5 mm. The present study showed that using 100%-ASIR on clinical routine-dose CT significantly improved detection sensitivity for CAD. However, the mean number of false-positive findings per scan increased significantly with increasing degree of ASIR. This may be largely due to the effect of edge enhancement in the HD-bone reconstruction kernel used in our study and to the decrease in image noise resulting from use of the ASIR. In general, performance in lesion-detection tasks and the accuracy of quantitative image-analysis tasks depends on the ultimate choice in reconstruction algorithm [21], and the CAD performance is influenced by the CT reconstruction algorithm [22]. In using CAD, a high-spatial-frequency algorithm is more appropriate for nodule detection than a standard algorithm, particularly with small nodules. In other words, a high-spatial-frequency algorithm such as the HD-bone reconstruction kernel produces much less smoothing and sharpens the resolution of small structures despite an increase in visible noise [23], and the use of ASIR further enhances the sharpness of the margins of tiny and faint CT findings, including GGO, as signal-to-noise ratio is improved by visually and quantitatively reducing image noise [3–8]. Consequently, these effects must improve not only the visualization of small structures [3,6,7], but